### THREE-PHASE CONTROLLED EXPANSION

#### SUPERALLOYS WITH OXIDATION RESISTANCE

K.A. Heck, D.F. Smith, M. A. Holderby and J.S. Smith

Research and Development Dept.

INCO ALLOYS INTERNATIONAL, INC. Huntington, WV

#### Abstract

Due to their low coefficients of thermal expansion, INCOLOY® alloys 903, 907 and 909 have contributed to improved efficiency in many aircraft engines designed since the mid '70's. The application of these Cr-free superalloys was, however, limited by inadequate oxygen environment resistance. The alloys were susceptible to both general oxidation and SAGBO (Stress Accelerated Grain Boundary Oxygen) embrittlement. Until just recently development efforts had focused on improving SAGBO resistance, but had ignored general oxidation resistance.

This paper reviews the status of a major, ongoing alloy research program on a new, low CTE superalloy system with improved environmental resistance. While early experiments confirmed that Al-containing alloys were extremely prone to SAGBO (as were alloys 903 with 1% Al and the intermetallic Ni<sub>3</sub>Al), continued research led to the unexpected discovery of a dramatic improvement in SAGBO resistance as Al exceeded 5%.\* This improvement was associated with the appearance of an Al-rich BCC phase ( $\beta$ ). The resulting development of this three-phase ( $\gamma$ - $\gamma$ '- $\beta$ ) alloy system is described, and numerous metallurgical challenges are addressed. The system's phase balance and properties are shown to be strongly dependent on the matrix elements as well as Al. Solutions to  $\beta$  phase anisotropy include control of Al and thermomechanical processing (TMP). An unexpected instability at "intermediate" temperatures (450°C-650°C) is correlated with Fe, Ti and Nb content.

The production and evaluation of two commercial–scale compositions demonstrate the feasibility of manufacturing alloys within this system. Development goals for improved oxidation resistance, SAGBO resistance, and strength are achieved in the composition currently designated as Exp. alloy 4005. These properties are combined with a low CTE (≥20% below that of INCONEL® alloy 718) and low density (≥ 5% lower than existing low CTE alloys). A new family of alloys could evolve from this research.

®INCOLOY and INCONEL are trademarks of the INCO family of companies.

Superalloys 1992 Edited by S.D. Antolovich, R.W. Stusrud, R.A. MacKay, D.L. Anton, T. Khan, R.D. Kissinger, D.L. Klarstrom The Minerals, Metals & Materials Society, 1992

<sup>\*</sup> Compositions shown are in weight % unless stated otherwise.

### Introduction

## Background

Chromium–free Fe–Ni–Co superalloys, INCOLOY alloys 903, 907 and 909, with coefficients of thermal expansion (CTE) 40% to 50% lower than conventional superalloys, have contributed to improved gas turbine efficiency in many aircraft engines manufactured since the mid '70's. Designs using these materials have provided a simple, effective means to attain significant gains in performance by controlling clearances between turbine or compressor blade tips and outer seals and shrouds. However, applications requiring service up to 650°C showed these alloys were vulnerable to two forms of oxygen environment attack: general oxidation and SAGBO.<sup>(1)</sup>

Numerous alloys and intermetallics are subject to SAGBO, wherein oxygen diffusion along grain boundaries results in intergranular failure and low ductility or life at temperatures of about 500°C or higher. (2,3) Traditional measures of SAGBO include high temperature tensile tests, notched bar stress rupture tests, and static or long dwell time fatigue crack growth tests. Sensitive materials can show the phenomenon as poor high temperature tensile ductility. More resistant materials, such as INCONEL alloy 718, show SAGBO via increased crack growth rates in air versus vacuum. (4)

Through the 70's and 80's, incremental improvements in the subject alloy system focused on improving SAGBO resistance, but did not address the improved general oxidation resistance required for future jet engine applications. Improving this characteristic of low CTE alloys is a difficult challenge since Cr and Al, the two alloying additions most effective for oxidation resistance, were found to have serious side effects:

- 1. Cr at levels sufficient for oxidation resistance (≥5%) degraded CTE performance by lowering the inflection or Curie temperature. (¹)
- 2. Al was associated with poor SAGBO resistance as demonstrated by (a) the stress rupture notch sensitivity in alloy 903 (with  $\sim 1\%$  Al)<sup>(5,6)</sup> and (b) the poor high temperature ductility of Ni<sub>3</sub>Al (despite its excellent oxidation resistance).<sup>(3)</sup>

### **Experimental Procedure and Technique**

The results that follow represent a small portion of work performed in the early stages of an ongoing alloy development. While initial discoveries were of great academic interest, it was also recognized that the developmental process would most quickly satisfy an existing need if the concept of concurrent engineering was applied. This approach required frequent customer input and large-scale production feasibility studies when milestones were reached.

Numerous vacuum induction ingots (22 kg–100mm  $\phi$ ) were cast, homogenized, and hot rolled (HR) to 17mm  $\phi$  bar. Unless otherwise noted, all specimens were annealed + aged accordingly: 1038°C/1–2h, air cooled (AC) + 760°C/16h, AC. Mechanical property evaluations included conventional room and elevated temperature tensile tests, 538°C/827MPa  $K_t$ =2.0 notch bar and 649°C/510 MPa combination smooth/ $K_t$ =3.6 notch bar stress rupture tests (SRU). CTE was measured in accordance with ASTM E228. Cyclic oxidation tests were performed at 704°C.

Microstructural analyses involved optical, TEM, X-ray diffraction (XRD), and SEM/EDX techniques. Optical samples were mounted longitudinally, polished, then immersion/stain etched in 100ml hot water + 50ml HCl + 0.5g K<sub>2</sub>S<sub>2</sub>O<sub>5</sub> + 5 drops HNO<sub>3</sub>, or electrolytically etched in 5% HCl + 95% methanol at 10 volts. TEM specimens were prepared by jet thinning with 10% HClO<sub>4</sub> + 90% methanol at -35°C and 30volts/125mA. XRD was performed on electropolished samples and H<sub>3</sub>PO<sub>4</sub> electrochemical extractions. SEM/EDX was performed on bulk samples.

### **Results & Discussion**

# **Discovery of Aluminum Effect**

High Temperature Properties: Despite the potential SAGBO problems associated with high AI, a factorial study of a 42% Ni, 18 %Co, balance Fe alloy was designed to determine the effect of AI (2.5% and 4%), Ti (1% and 2%) and Nb (2% and 3%). While all of these alloys had excellent oxidation resistance, they were brittle when tensile tested at 760°C. The example selected in Figure 1 confirms this embrittlement was a result of SAGBO.

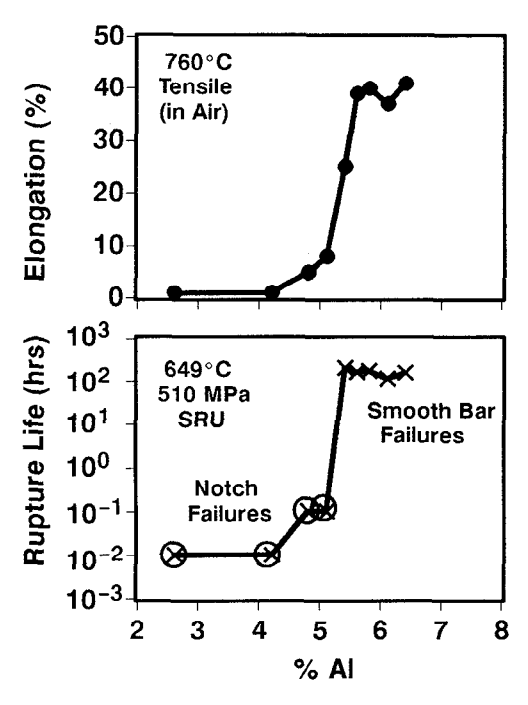


Figure 2. Effect of Al on tensile ductility and stress rupture life.

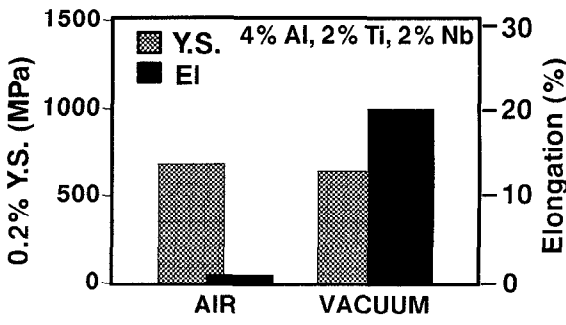


Figure 1. Effect of atmosphere on 760°C tensile properties.

Additional study heats with Al  $\geq$  4% (3% Nb and 1.5% Ti) led to the unexpected discovery, in Figure 2 (top), that 760°C tensile ductility dramatically improved as Al exceeded 5%. This improvement came without any loss in strength (0.2% YS~830 MPa). Figure 2 (bottom) verifies the improvement in SAGBO resistance as measured by 649°C/510 MPa combination bar rupture tests. Rupture ductilities of smooth bar failures were >25%.

Structure of  $\gamma$ – $\gamma$ '– $\beta$  Alloys: The explanation for this AI effect is demonstrated in Figures 3 and 4 which compare the microstructures and bulk sample XRD patterns of the 4.8% and 5.6% AI alloys that straddle the transition from notch brittle to notch ductile behavior. The lower AI material had coarse grains with clean grain boundaries. The higher AI alloy had a fine duplex structure of austenitic grains and a globular to angular BCC phase identified in Figure 4 (bottom).

The Fe-Ni-Al ternary diagram<sup>(7)</sup> in Figure 5 helps explain this dramatic change in microstructure. A transition from the  $\gamma+\gamma'$ , typical of most superalloys, to the  $\gamma+\gamma'+\beta$  phase field occurs at intermediate temperatures as Al is increased in a Ni-Fe based alloy (assuming 42% Ni + 18% Co = 60% Ni). The  $\beta$  phase is a Ni-Al-rich BCC phase that has since been identified in alloy compositions with good SAGBO resistance. Spectrographic analysis of the base alloy is compared to semi-quantitative EDX analyses in Table I.  $\beta$  particles contained significant amounts of Fe and Co and less than 50 at % Al. The composition is actually closer to A<sub>2</sub>B or A<sub>3</sub>B than to AB (A = Ni, Fe, Co B = Al), with Co content nearly the same as in the matrix. While indications of B2 ordering were found, the off-stochiometric composition suggests that other order/disorder phenomena might occur in the particles depending upon heat treatment.<sup>(8,9)</sup> Fine, Ni-enriched  $\gamma'$  with L1<sub>2</sub> structure has been electrochemically extracted from all alloys in this Al-series.

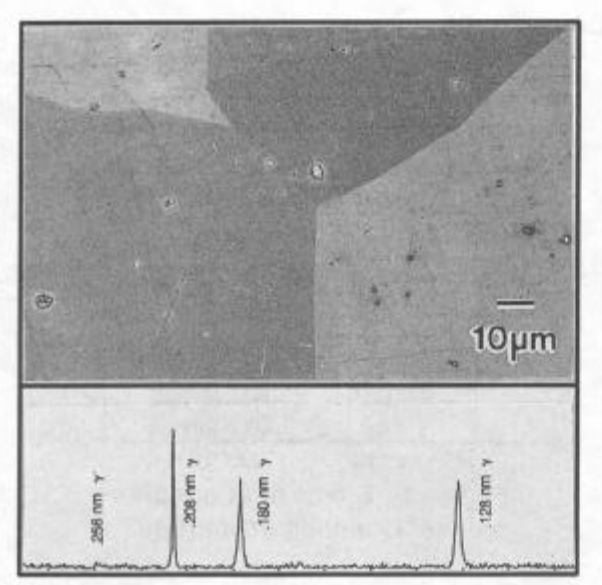


Figure 3. Structure & phases: 4.8% Al alloy

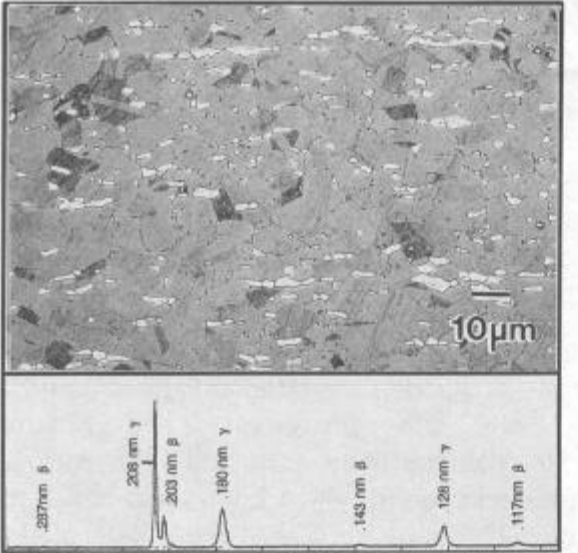


Figure 4. Structure & phases: 5.6% Al alloy

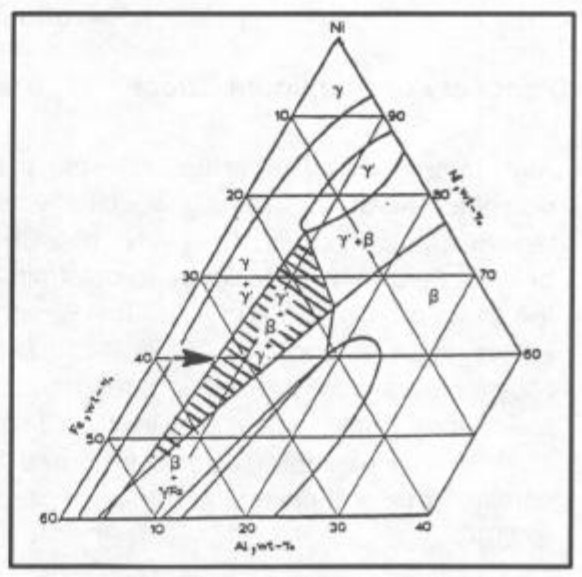


Figure 5. Portion of Fe-Ni-Al 750°C ternary<sup>(7)</sup>

Table I. Phase Compositions

		Ni	Fe	Co	AI*	Nb*	Ti
Base	W%	42	29	18	6	3	1.4
	At%	39	29	17	12	1.8	1.7
Matrix + γ'	W%	39	33	18	7	2.3	1.2
	At%	35	31	17	14	1.4	1.3
всс	W%	44	21	15	17	1.5	1.7
	At%	36	19	13	30	0.8	1.8

\*Note: Analytical discrepancy between spectrographic and EDX results.

# First Large-Scale Melt

Although much optimization work remained, it was decided to determine the commercial feasibility of producing a high aluminum, three-phase alloy. Areas of major concern included: (1) potential segregation (would the alloy be subject interdendritic Nb segregation and/or Al-rich primary  $\gamma'$  formation?); (2) hot workability (would the alloy have a narrow hot working range typical of high Al two-phase alloys?); (3) weldability (would the alloy be totally unweldable, could cast structures be welded for electrode stubbing?). To address such issues, a 14,500 kg vacuum induction melt (VIM) with a composition of 42% Ni, 29.5% Fe, 18% Co, 6% Al, 3% Nb, 1.5% Ti was cast as electrodes for vacuum arc remelting (VAR) and electroslag remelting (ESR). Ingots ranging from 380 mm to 508 mm  $\varphi$ , were processed to a variety of products including forged billet, extruded rectangle and cold-rolled sheet. Processing was largely based upon procedures established for existing superalloys, such as alloy 718. Production problems encountered were not insurmountable. The alloy was easier to work and weld than many other high Al superalloys. This characteristic was attributed to the effects of  $\beta$  phase (which is ductile at high temperatures) and high Co content  $\cdot$ 

Figure 6 demonstrates that gas turbine rings measuring 635mm ID x 700mm OD x 100mm high were successfully manufactured using conventional processing techniques. This early commitment to commercial scale-up proved invaluable and validated this three-phase alloy technology.

## Anistropy

These rings had a uniform, fine grained matrix (20 µm), but had an anisotropic independently recrystallized B structure as shown in Figure 7. The ternary liquidus-solidus projection for Fe-Ni-Al (7) and for Co-Ni-Al(11) shows a y-B eutectic valley exists roughly parallel to constant Al within the composition ranges of interest. Homogenization studies showed it difficult to fully solution the interdendritic phases in a 6% Al alloy without serious incipient melting problems. thought that anisotropy could be reduced by lowering Al away from the high melting point (β) side of this eutectic. Figure 8 confirms that lowering Al did reduce the primary or interdendritic phases in the cast structure. In lower Al alloys, these phases can then be solutioned by a more economical homogenization practice.



Figure 6. Hot rolled gas turbine rings.

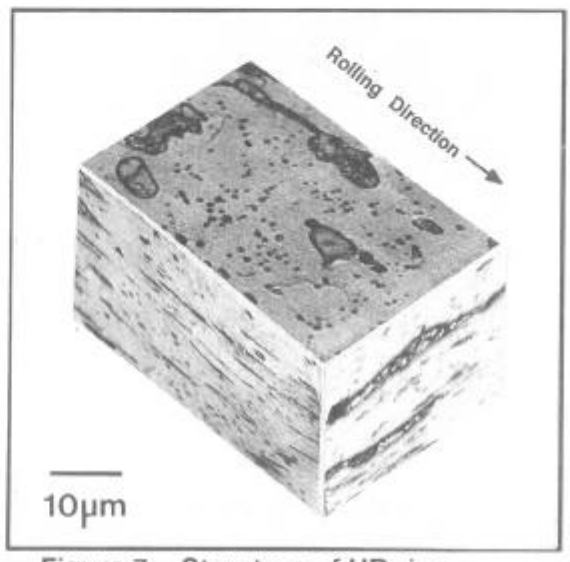
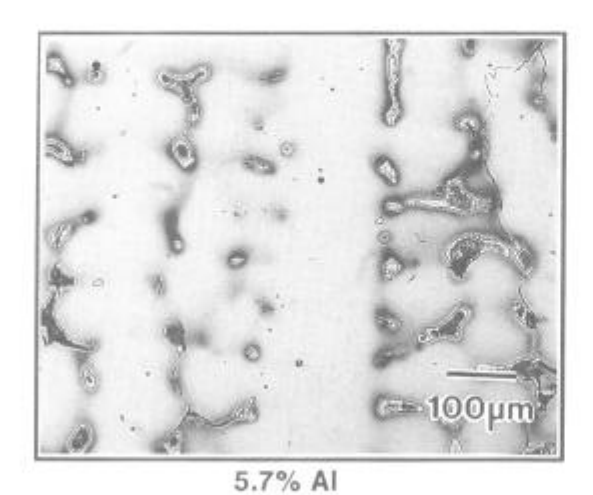


Figure 7. Structure of HR ring.

Before fine–grained structures could be obtained with lower Al content, the hot working practice had to be adjusted to provide recrystallization energy below the lowered  $\beta$  solvus. Figure 9 shows that a fine grained, more isotropic structure was achieved by combining composition and TMP controls. Isotropy was further improved by controlling sub–solvus work and subsequent annealing.



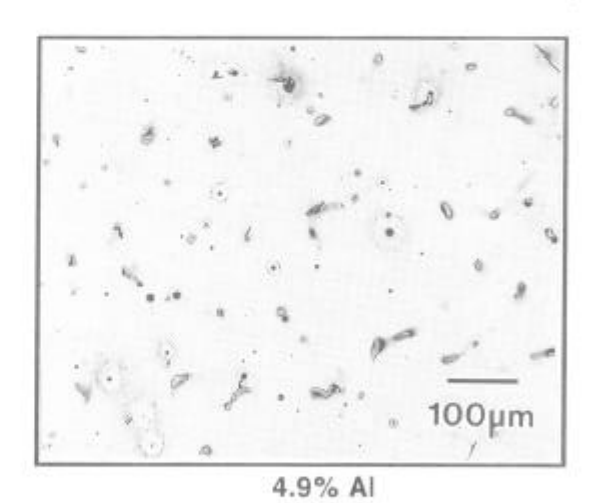
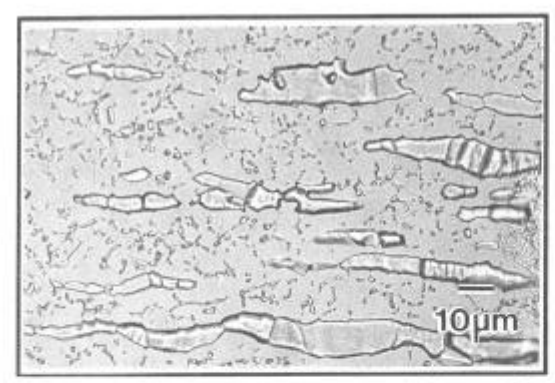
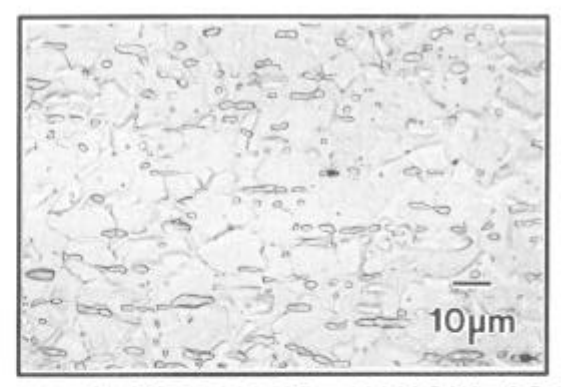


Figure 8. The effect of Al on as-cast microstructure.





6% AI: HR @ 1177°C+1038°C/1h, AC

5. 2% Al: HR @ 1065°C+1038°C/1h, AC

Figure 9. The effect of Al and TMP on microstructure.

### Fe-Ni-Co Effects

Changing the Fe, Ni, or Co contents of current y'-strengthened low CTE superalloys primarily affects physical properties (i.e., CTE, modulus, etc.). However, in this new alloy system, these elements also determine the phase balance and resulting mechanical properties. These effects are illustrated below for alloys containing 6% AI, 3% Nb and 1.5% Ti.

The 3–D response surface in Figure 10 (left), correlating 649°C tensile elongation (a rough indicator of SAGBO sensitivity) with the transition elements, shows that ductility was improved significantly as Ni was decreased. The low ductility (<10%) found in the earlier 42% Ni, 29.5% Fe, 18% Co alloy could be raised appreciably by increasing the Co/Ni ratio. Microstructural analyses showed that alloys with increased Fe or Co (decreased Ni) had increased volume fractions of  $\beta$ . Figure 10 (right) underscores the complex relationship between these elements and those phases affecting SAGBO performance and strength, as measured by 649°C/510 MPa SRU life. Compositions with high Ni, that formed little or no  $\beta$ , failed quickly in the notch. Alloys with lower Ni failed in the smooth bar. Life decreased as Fe exceeded 25%, and ductile tensile failures occurred as Fe exceeded 35%. The high Fe alloys had large volume fractions of  $\beta$  in  $\gamma$  matrices with little  $\gamma'$ . This response surface shifted as Al was lowered (i.e., to reduce anisotropy).

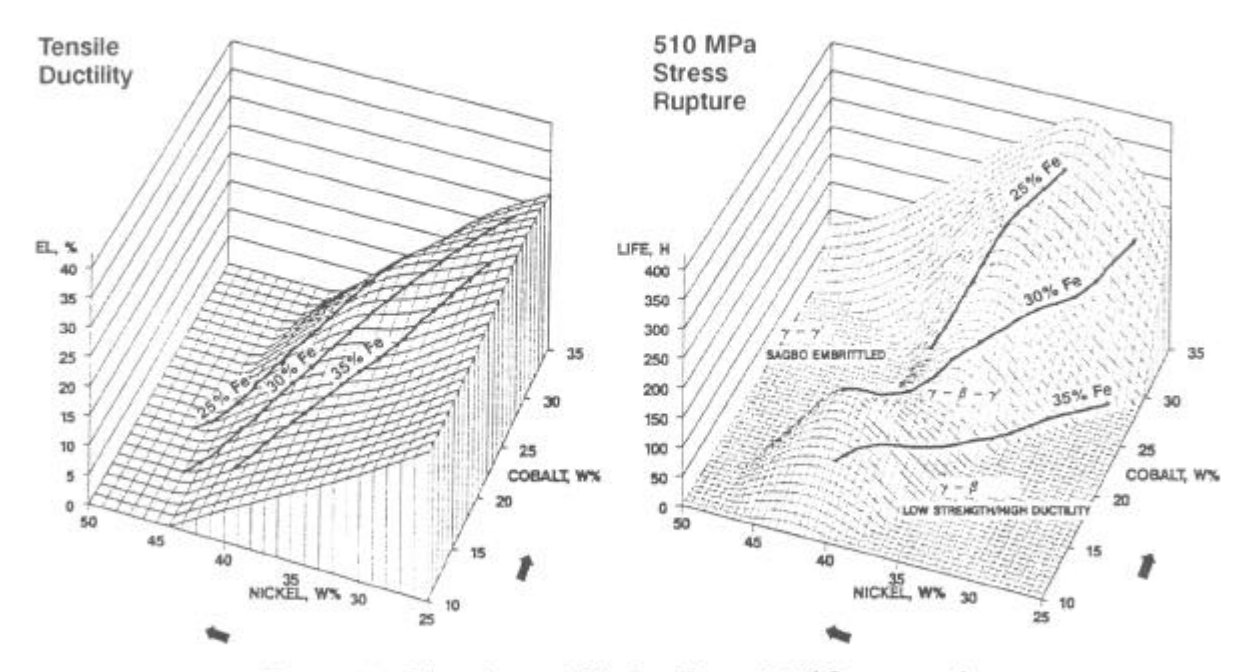


Figure 10. The effect of Ni-Co-Fe on 649°C properties.

These data indicated that alloys in this system possess notch ductility (resistance to SAGBO) largely because  $\beta$  phase is more ductile than the very strong  $\gamma$ ' strengthened matrix at intermediate temperatures. Grain boundary stress relaxation at the micro-level makes the bulk alloy resistant to cracking. (12) The excessive precipitation of  $\beta$  accompanied by the loss of  $\gamma$ ' strengthening lowers high temperature strength and creep resistance (typical of BCC  $\beta$ ). (13)

The design of this new alloy must include consideration for the effects of Fe, Ni and Co on CTE as well as the phase/mechanical property effects just discussed. Since Fe plays the dominant role in determining CTE, it would seem that Fe content could be established on the basis of CTE and desired SAGBO resistance (to guarantee adequate  $\beta$ ). However, as will be shown below, Fe can have a detrimental effect unanticipated in this original alloy development.

## **Intermediate Temperature Stability:**

It was found that some compositions with the desired structures and properties were metastable at temperatures from 450°C to 650°C. The results of two factorial studies have been selected to illustrate this phenomenon: a) a study of Fe and Ni in alloys containing 5.4% Al, 3% Nb, 1.4% Ti (bal Co); and b) a study of Nb and Ti in alloys containing 30% Fe, 34% Ni, 5.4% Al (bal Co).

**Fe-Ni Study:** The results in Table II (top) demonstrate that all alloys had good strength and ductility in the annealed and aged condition, and that yield strength increased somewhat as Fe or Ni were increased (Co was decreased). However, Table II (bottom) shows that an additional exposure at 592°C/100h:

- 1. strengthened 25% Fe alloys while lowering ductility;
- 2. embrittled alloys containing 30% and 35% Fe such that tensile specimens failed in machined threads.<sup>†</sup>

**Nb-Ti Study:** Annealed + aged data in Table III (top) reveal that these alloys had very good ductility and that, as expected, they were strengthened by increased Nb and Ti. Table III (bottom) shows that 592°C/100h exposure:

- 1. increased yield strengths of the Nbfree alloys by ≥100% (to ≥1400 MPa) while lowering ductilities to only 2-5%;<sup>†</sup>
- 2. increased yield strengths of Nb-con taining alloys by 10 to 30%;
- 3. lowered ductilities considerably in alloys with  $Ti \ge 0.8\%$ .

Table II. Effect of Ni-Fe on Room Temperature Tensile Properties

Tomporataro Tomono i Toportico						
*0.2% Y BIT = broke	34% Ni	37% Ni	40% Ni			
Annealed	25% Fe	YS*: EI%:	965 21		1020 20	
+	30% Fe	YS*: EI%:	1041 19	1062 19	1103 18	
Aged	35% Fe	YS*: EI%:	1069 20		1131 19	
Annealed	25% Fe	YS*: EI%:	1165 16		1165 13	
+ Aged	30% Fe	YS*: EI%:	BIT	BIT	ВІТ	
+ 592°C/100h	35% Fe	YS*: EI%:	BIT		BIT	

Table III. Effect of Nb-Ti on Room Temperature Tensile Properties

remperature remainer roperties						
*0.2% Y	0.2	0.8	1.4			
	% Ti	% Ti	% Ti			
Annealed	0%	YS*:	490	710	807	
	Nb	EI%:	32	26	23	
+	1.5%	YS*:	696	848	965	
	Nb	EI%:	25	23	20	
Aged	3.0%	YS*:	896	1048	1103	
	Nb	EI%:	24	19	25	
Annealed	0%	YS*:	1420	1572	1510	
	Nb	EI%:	5	2	2	
+	1.5%	YS*:	883	1007	1172	
Aged	Nb	El%:	19	18	12	
+	3.0%	YS*:	1083	1172	1234	
592°C/100h	<b>N</b> b	EI%:	25	11	1	

<sup>†</sup>Note: Ground threads gave better measurements in the low ductility range for Nb-Ti study.

Structure Effects: The previous studies demonstrated that some Nb is required in this alloy system and that both Ti and Fe must be tightly controlled. These effects were characterized by optical metallography, XRD, SEM, and TEM analyses. The latter, high magnification, analysis was most effective in revealing the complexity of this phenomenon.

Figure 11 shows a structure typical of annealed + aged alloys with good mechanical properties. A profuse precipitation of somewhat rounded  $\gamma'$  (without denuded zones) is accompanied by large  $\beta$  particles. A stable alloy will retain this structure after exposure. Discontinuous precipitation was noted in the grain boundaries of many specimens.

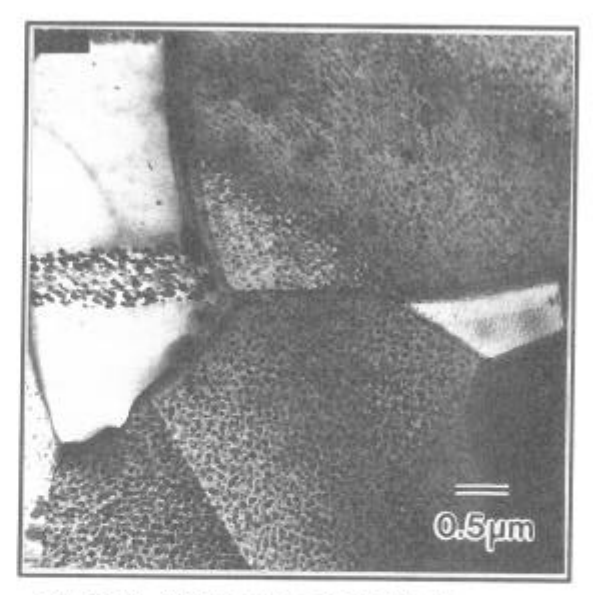


Figure 11. TEM image of ductile alloy.

In general, two types of  $\beta$  phase have been observed by TEM: one featureless (except for its "tweed" appearance)<sup>(14)</sup> and another that contains structural features such as fine spherical, cuboidal or acicular (at higher aging temperatures) precipitates.

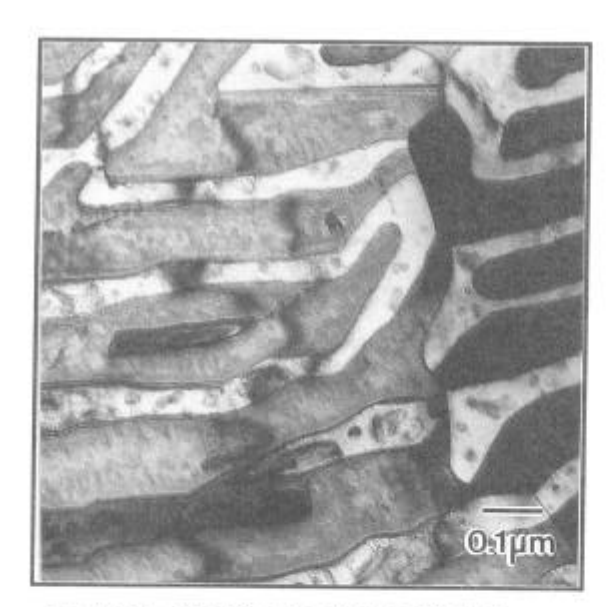


Figure 12. TEM image of embrittled Nbfree alloy.

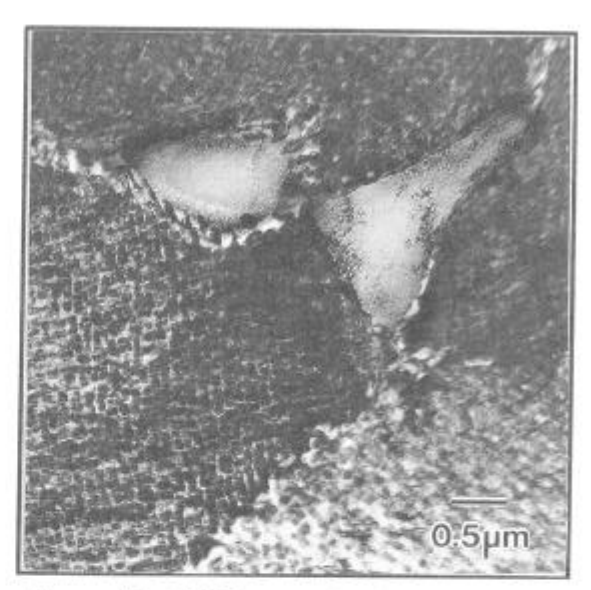


Figure 13. TEM image of embrittled 1.4% Ti, 30% Fe alloy.

There are numerous structural features associated with intermediate temperature embrittlement. At the Nb-free extreme, the XRD and TEM in Figure 12 reveal a eutectoid decomposition occurred, forming fine lamella of BCC and FCC ( $\gamma'$ ) phases (barely resolvable optically). Embrittlement of a high Ti, high Fe alloy is correlated, in Figure 13, with a Ti, Nb-enriched interfacial ( $\gamma$ - $\beta$ ) phase, as well as with fine particles precipitated within the  $\beta$  phase. The matrix between  $\gamma'$  particles displays a high defect density after exposure, contributing to a dramatic increase in hardness. Ti and Nb also affect the  $\gamma'$  morphology and  $\gamma$ - $\gamma'$  mismatch. The numerous phases and the fine scale of the microstructural changes dictate the need for convergent beam TEM to better understand the complex nature of these alloys.

# Second Large-Scale Melt

In consideration of the findings in the previous three sections, a second commercial feasibility melt was produced with a nominal composition of 33% Ni, 31% Co, 27% Fe, 5.3% Al, 3% Nb and 0.6% Ti. The 9,100 kg VIM melt was cast to electrodes which were VAR remelted into respective 508 mm  $\varphi$  and 380 mm  $\varphi$  ingots. Based on the experience with the first large–scale heat, process modifications led to the successful manufacture of a variety of products including hot–rolled rings, hot–rolled flats and cold–worked sheet in thicknesses from 0.6 to 2.5 mm (1 m width).

Table IV. Tensile Properties of 2nd Large-Scale Melt (Ring Section)

Test Temp.	Orien- tation	Y.S. (MPa)	T.S. (MPa)	EI (%)	R.A. (%)
75°C	Tang.*	1048	1303	18	44
	Axial	1062	1317	18	37
	Radial	1048	1289	14	28
538°C	Tang.*	834	1145	14	37
	Axial	883	1145	13	31
	Radial	876	1131	9	19

<sup>\*</sup>Average of 6 tests.

Heat Treatment: 1010°C/1 h, AC + 775°C/12 h, furnace cooled (55°C/h) to 620°C/8 h, AC

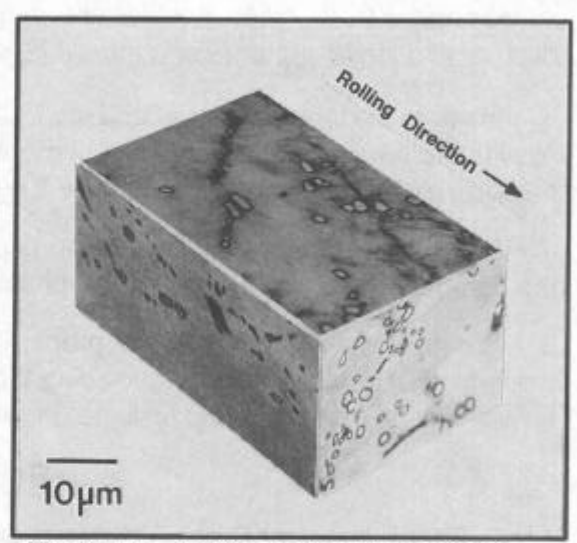


Figure 14. Isotropic structure of hot rolled + heat treated ring.

The tensile properties in Table IV and the microstructures in Figure 14, from a gas turbine ring of relatively large cross section (416mm ID X 556mm OD X 175 mm), demonstrated that alloys in this three–phase system can be manufactured with useful engineering properties and minimal anisotropy. SAGBO resistance, as measured by 538°C notched bar rupture tests, was very good (tangential and axial rupture lives exceeded 200 hours). Figure 15 shows this alloy's CTE characteristic to be ≥20% below that of alloy 718, while Figure 16 confirms its excellent oxidation resistance compared to that of alloy 909. Lastly, this system appears capable of combining high temperature strength, low CTE, SAGBO and oxidation resistance without sacrifice to the critical property of density (i.e., the ρ of this alloy is 5–6% lower than that of alloys 909 and 718).

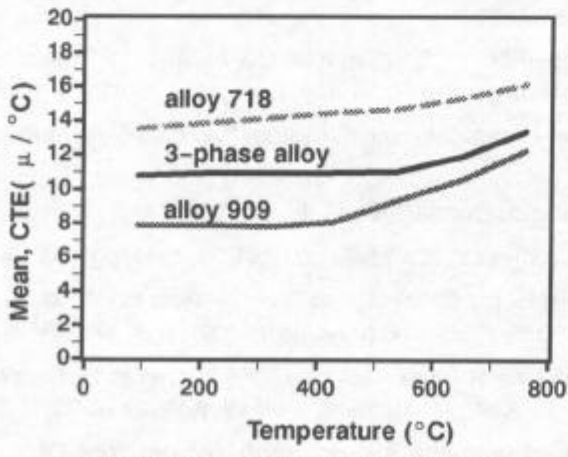


Figure 15. CTE Comparisons

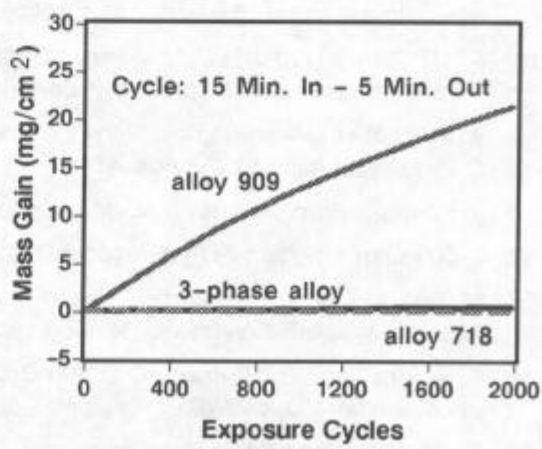


Figure 16. 704°C Cyclic Oxidation

## **Summary**

- 1. Al had a significant influence on the environmental resistance, properties and phase equilibria of low CTE Ni–Fe–Co superalloys. Alloys containing Al above 5% precipitated an Al–rich BCC  $\beta$  phase which resulted in unexpectedly good SAGBO resistance. Alloys containing Al less than 5.6% showed acceptable isotropy in a fine–grain structure when processed with controlled TMP.
- 2. The phase balance and properties of these  $\gamma$ - $\gamma$ '- $\beta$  alloys were also dependent upon the ratios of Ni, Fe and Co. High temperature ductility and stress rupture properties were improved by increasing the Co/Ni ratio. Besides affecting CTE, Fe had a marked effect on high temperature ductility and stress rupture performance (SAGBO) because it stabilized  $\beta$  phase.
- 3. Intermediate temperature (450°C-650°C) stability was influenced by Fe, Ti and Nb content. Available data suggest that Fe and Ti should be controlled to levels below 30% and 0.80% respectively. Nb prevented embrittlement by stabilizing the three-phase structure.
- 4. The successful production of a variety of products from two large-scale melts demonstrated the commercial feasibility of this three-phase system currently designated as Exp. alloy 4005.
- 5. This new system combines the property advantages of two intermetallic phases within a workable FCC matrix, thereby providing the potential for low CTE superalloys with improved environmental resistance and lowered density.

#### References

- D. F. Smith and J. S. Smith, "A History of Controlled, Low Thermal Expansion Superalloys," *Physical Metallurgy of Controlled Expansion Invar-Type Alloys*, ed, K. C. Russell and D. F. Smith, 1989, pg. 253–272.
- 2. D. A. Woodford and R. H. Bricknell, "Environmental Embrittlement of High Temperature Alloys by Oxygen," *Treatise on Materials Science and Technology*, Academic Press, vol. 25, 1983.
- 3 C. T. Liu and C. L. White, "Dynamic Embrittlement of Boron-Doped Ni<sub>3</sub>Al Alloys at 600°C," *Acta Metallurgica, Vol 35, No. 3, 1987, pgs. 643–649.*
- 4. K. M. Chang, "Metallurgical Control of Fatigue Crack Propagation in Alloy 718," *Superalloys 718, 625 and Various Derivatives*, ed., E. A. Loria, 1991, pgs. 447–456.
- 5. D. F. Smith and D. E. Wenschhof, "Effects of Test Atmosphere and Thermo–Mechanical Processing on the Stress–Rupture Properties of INCOLOY alloy 903," (unpublished paper presented at the Materials Science Symposium, 1974, Detroit, Michigan).
- 6. H. W. Carpenter, "Alloy 903 Helps Space Shuttle Fly," Metals Progress (August 1976), pgs. 25-29.
- 7. V. G. Rivlin and G. V. Raynor, "Critical Evaluation of Constitution of Aluminium–Iron–Nickel System," *International Metals Review*, Vol. 3, 1980, pgs. 79–93.
- 8. A. J. Schwartz and W. A. Soffa, "Decomposition of Beta-Phase Co-Al Alloys: Precipitate Crystallography and Morphology," *Scripta Metallurgica et Materialia*, (Jan. 1991) Vol 25, pg. 185.
- 9. A. J. Bradley, "Microscopical Studies on the Iron-Nickel-Aluminium System," *Journal of the Iron and Steel Institute* (May 1952), pgs. 41–47.
- 10. J. Heslop, "Proc. Journées Int. des Applications du Cobalt", Brussels, pg. 209.
- 11. J. Schramm, "The Ternary System Nickel-Cobalt-Aluminum", Z. Metallkunde, Vol. 33, 1941, pgs. 430-412.
- 12. M. Welker et. al., "Creep Crack Growth of Materials for the Chemical and Petrochemical Industries," *Heat Resistant Materials Conference Proceedings*, ed. D. J. Tillack and K. Natesan, 1991, pgs. 477–484.
- 13. P. R. Strutt and B. H. Kear, "Creep in Ordered Nickel Base Alloys," *High-Temperature Ordered Intermetallic Alloys, MRS Proceedings*, ed. C. C. Koch et. al., 1985, Vol. 39, pgs. 279–292.
- 14. C. M. Wayman, "Modulated Microstructures in β-Phase Alloys," *High-Temperature Ordered Intermetallic Alloys*, *MRS Proceedings*, ed. C. C. Koch et. al., 1985, Vol. 39, pgs. 77–91.